MRST-Shale: an open-source framework for generic numerical modeling of unconventional shale and tight gas reservoirs

Bin Wang, Femi Olorode, Feng Yin, Chenyong Li

Abstract

Numerical modeling technique plays a critical role in providing an essential tool for evaluating, optimizing the development of shale gas in unconventional reservoirs. It is still challenge to model and understanding the flow behavior in such complex system with multi-scale fracture networks and complex transport mechanisms. In this paper, a generic shale gas transport model is developed using embedded discrete fracture model (EDFM) to model shale gas flow behavior in fractured shale reservoir. A general open-source simulator MRST-Shale is also developed based on MATLAB Reservoir Simulation Toolbox (MRST) with state-of-art flow mechanics. The simulator is intended for providing a powerful and flexible tool to evaluate shale gas production with arbitrary flow mechanism and fracture networks topology. MRST-Shale is verified against several open-source, commercial and in-house reservoir simulators. To show the applicability of MRST-Shale, example field applications of history matching and production forecasting and sensitivity analysis of new geomechanics model as well as multi-scale fractures are also illustrated.

Source code is available at https://github.com/BinWang0213/MRST-Shale

Key words: Shale gas; MRST; embedded discrete fracture model; Open-source implementation

1 Introduction

Advances in formation stimulation technology are promoting global interest in the recovery of hydrocarbons from tight and shale gas reservoirs. Numerical modeling will continue to play a critical role toward the evaluation, design and management of stimulation and production processes.

Gas transport in shale formation involves complex gas transport mechanisms due to the presence of a large amount of nanopores and organic matter, which include gas desorption, adsorbed gas porosity, gas slippage, and Knudsen diffusion, etc (Javadpour et al, 2007; Wang and Reed, 2009; Civan et al, 2010,2011; Sakhaee and Bryant, 2012; Akkutlu and Fathi, 2012 and Yu et al, 2016). In addition, the fractured shale matrix is comprised of a hierarchical network of pores down to a few nanometers, cracks and micro-fractures, which makes the formation a multi-scale porous medium with large heterogeneity and anisotropy (Akkutlu et al, 2018). Hence, the complex gas transport mechanisms and multiscale fracture system (Fig. 1) pose a great challenge to accurately and efficiently evaluate and simulate well performance in shale gas reservoirs.

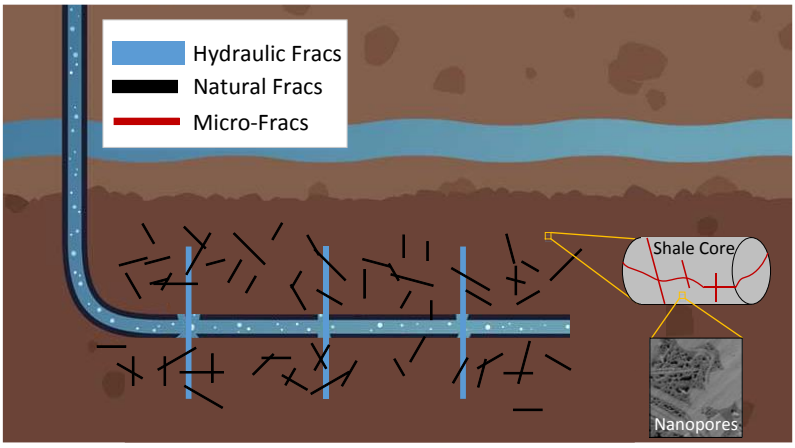

Figure 1 – Multi-scale natural of shale gas production

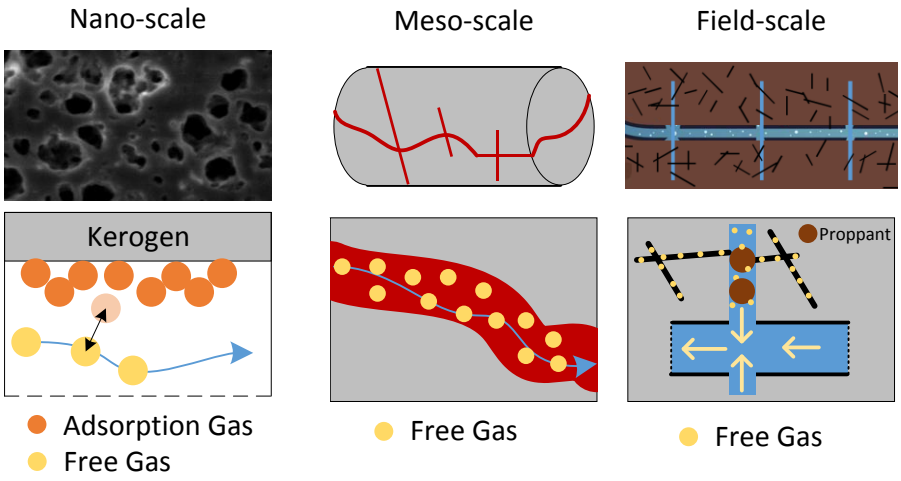

Figure 2 – Multi-scale shale gas storage and transport

In recent years, considerable efforts have been made to model well performance from shale reservoirs with complex fracture geometry analytically, semi-analytically or numerically. For the analytical-based method (Chen et al, 2016 and Yang et al, 2017), it is difficult to fully capture the complex physics existed in shale gas reservoirs such as heterogeneity, multiphase flow (gas/water), pressure-dependent rock properties and fracture conductivity. For the numerical-based method (Sandve et al, 2012 and Olorode et al, 2013), many efforts have been made by using unstructured gridding with local refinement near the fractures to capture the true complex fracture geometry and nonlinear physics. However, the unstructured grids are still challenging to use efficiently in the field scale due to very complicated gridding issues and an expensive computational cost. To overcome the above issues, a state-of-the-art embedded discrete fracture model (EDFM) was developed. In EDFM, the complex fractures are embedded in conventional structured matrix grids explicitly without the need of LGR in the vicinity of fractures. This approach is simpler and faster to capture the complex

fracture geometries (Xu, 2015 and Olorode et al, 2017).

Although there are many existing numerical models for shale gas simulation, many of the complex phenomenon have not been completely analyzed, and these models are implemented in in-house simulators or commercial simulators. Hence, it is necessary to develop a comprehensive and open-source simulator to fill this gap.

In this paper, we present a generic governing equation for shale gas flow considering sorption, nanoflow mechanism, multi-scale fracture system and pressure-dependent matrix and fracture rock properties. An efficient numerical model based on EDFM is also implemented in a powerful open-source simulator (MRST) to simulate shale gas flow behavior and production performance. The developed simulator can handle nonpalanar hydraulic fractures and stochastic natural fractures with arbitrary fracture conductivity and aperture. The pressure-dependent fracture (including, hydraulic fractures, natural fractures and micro-fractures) conductivity are also considered. The implemented numerical model is verified against fully resolved in-house reservoir simulator and MRST with highly refined explicit fracture model. Finally, the effect of stochastic natural fracture, nanoflow mechanics, hydraulic fracture pattern, pressure-dependent matrix permeability, pressure-dependent fracture conductivity on production performance are investigated.

2 Mathematical equations

Considering the isothermal single-component single-phase gas flow in 2D fractured porous media with 1D fracture line without gravity effect. The general governing equation for shale gas flow in matrix (Ω_m), considering storage (m_{ad}) and transport mechanisms (F_{app}), can be expressed as follows:

$$\frac{\partial}{\partial t}\left(\rho_g\phi+(1-\phi)m_{ad}\right)+\nabla\cdot(-\rho_g\frac{\prod_i F_{app,i}k_0}{\mu_g}\nabla p)=\rho_g q_w \quad \text{in } \Omega_m \tag{1}$$

Similarly, the governing equation for fracture (Ω_f), only considering transport mechanisms, can be expressed as follows:

$$\frac{\partial}{\partial t}\left(\rho_g\phi\right)+\nabla\cdot(-\rho_g\frac{\prod_i F_{app,i}k_0}{\mu_g}\nabla p)=\rho_g q_w \quad \text{in } \Omega_f \tag{2}$$

Introducing inverse formation volume factor $b_g=\rho_g/\rho_{gsc}$ ($\rho_g=b_g\rho_{gsc}$), the above equation

can be rewritten as follows:

$$\begin{aligned}\frac{\partial}{\partial t}\left(b_g\phi+\frac{(1-\phi)}{\rho_{gsc}}m_{ad}\right)+\nabla\cdot(-b_g\frac{\prod_i F_{app,i}k_0}{\mu_g}\nabla p)=b_g q_w \quad \text{in } \Omega_m\\ \frac{\partial}{\partial t}\left(b_g\phi\right)+\nabla\cdot(-b_g\frac{\prod_i F_{app,i}k_0}{\mu_g}\nabla p)=b_g q_w \quad \text{in } \Omega_f\end{aligned} \tag{3}$$

where ρ_g is the mass density of gas, M/L^3; u_g is the viscosity of natural gas, N.T/L^2 m_{ad} is the accumulation term due to adsorption, M/L^3; ϕ is the matrix porosity, dimensionless; k_0 is the absolute Darcy permeability of the reservoir rock, L^2. $F_{app,i}$ is the i-th permeability correction factor for a specific shale gas transport mechanism; q_w is the volumetric sink/source term, M/L^3/T. k_0 is the absolute Darcy permeability of the reservoir rock, L^2.

2.1 Gas properties

Density: The pressure-dependent density of natural gas can be calculated by the real gas law:

$$\rho_g=\frac{pM}{Z(p,T)RT} \tag{4}$$

where M is the molecule weight of the natural gas, M/Mol; R is the Boltzmann constant, 8.314 ML^{2}T^{-2}/T/mole); T is the reservoir temperature, T;

The compressibility factor Z can be calculated using implicit Peng-Robinson equation-of-state (PR-EOS) equation or empirical explicit equation. Using the empirical equation, the complex natural gas mixture can be considered as a single component with pseudo-temperature and pseudo-pressure. Mahmoud (2013) developed an explicit empirical equation for natural gas mixture as follows:

$$Z(p,T)=0.702e^{-2.5T_{pr}}\cdot p_{pr}^2-5.524e^{-2.5T_{pr}}\cdot p_{pr}+(0.044T_{pr}^2-0.164T_{pr}+1.15) \tag{5}$$

where the pseudo-temperature and pseudo-pressure can be expressed as $T_{pr}=T/T_c$ and $p_{pr}=p/p_c$, respectively. T_c is the critical pressure and critical temperature for the shale gas mixture.

For single component gas simulation, such as methane, the Z factor can be accurately estimated by solving a cubic function of PR-EOS as follows (Lira and Elliott, 2012):

$$
\begin{aligned}
&Z^3 + a_2 Z^2 + a_1 Z + a_0 = 0 \\
&a_0(p,T) = (AB - B^2 - B^3),\ \ a_1(p,T) = A - 3B^2 - 2B,\ \ a_2(p,T) = B - 1 \\
&A = ap/(RT)^2,\ B = bp/(RT) \\
&a = \frac{0.457235 R^2 T_c^2}{p_c},\ \ b = \frac{0.0777961 RT_c}{p_c}
\end{aligned} \tag{6}
$$

In this paper, an analytical solution (see details in appendix B of Lira and Elliott, 2012) is used for solving the cubic equation. For more complex natural gas mixture, it requires complex flash calculation and belongs multi-component compositional simulation which will be investigated in our future work.

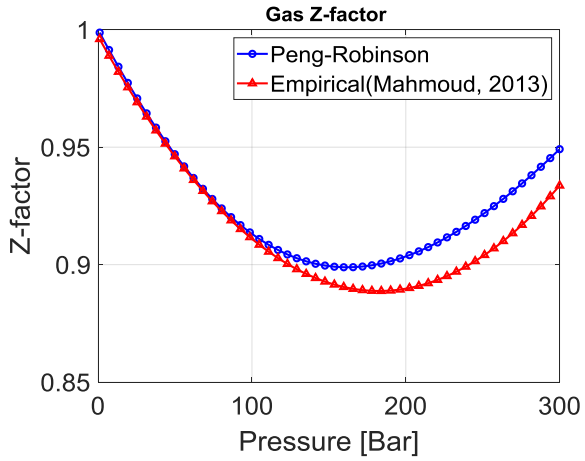

Fig. 4 Evaluated natural gas Z-factor for empirical and PR-EOS models with T=352 K, T_c=191 K, p_c=4.64 MPa, R=8.314 J/(K.mol)

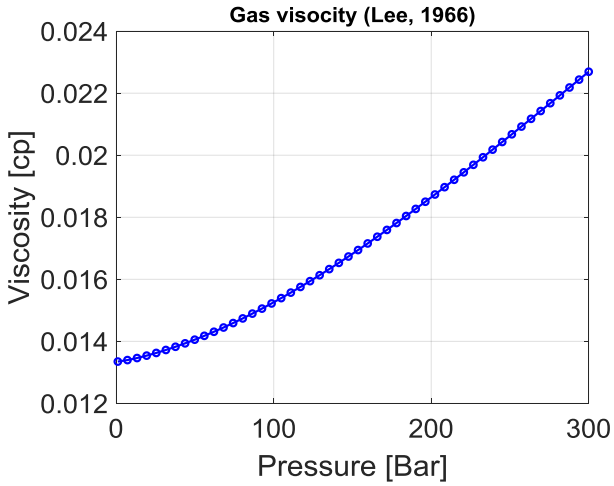

Fig. 5 Evaluated natural gas viscosity using Lee Lee-Gonzalez-Eakin empirical correlation with M=16.04 g/mol and T=633.6 Rankine

Viscosity: The density-dependent viscosity of shale gas can be estimated by

Lee-Gonzalez-Eakin empirical correlation (Lee et al, 1966) as follows:

$$\mu_g = 10^{-7} K \exp(X \rho_g^Y)$$
$$K = \frac{(9.379 + 0.01607M)T^{1.5}}{209.2 + 19.26M + T}, \quad X = 3.448 + \frac{986.4}{T} + 0.01009M, \quad Y = 2.447 - 0.2224X \tag{7}$$

where the unit of M, T are g/mol and Rankine, respectively.

Noted that the usage of pseudo-pressure can linearize the nonlinearity introduced by pressure-dependent gas viscosity and compressibility (Eqs. 5-6) but lead to large error especially for tight shale reservoir (Houze et al, 2010). Thus, in this paper, the real-gas equation with nonlinearity is used.

2.2 Transport and storage mechanism

Since rapid commercial development of unconventional tight reservoirs in recent years, many researchers spend enormous effort to understand the transport and storage mechanism of shale gas in such complex multi-scale system (**Fig. 4**). Main physical mechanisms (Yu et al, 2016; Klinkenberg, 1941; Florence et al, 2007; Javadpour, 2007; Civan, 2010) can be summarized as in **Table 1**.

For MRST-Shale, any mechanism model can be easily implemented by defining nonlinear gas storage function (m_{ad}) and permeability correction function (F_{app}). Several popular models are considered and implemented as follows:

Table 1. Key transport and storage mechanism for shale gas flow

Mechanism	Models	Type	Continuum
Adsorption	Langmuir, BET	S	Matrix
Slip flow & Diffusion	Klinkenberg, Florence, Javadpour, Civan	T	Matrix
Non-Darcy flow	Darcy-Forchheimer	T	Fracture

Adsorption: The gas molecules adsorbed in the pore wall of Kerogen in shale reservoir can be modeled using monolayer Langmuir isotherm and multiple layer BET isotherm as follows (Yu et al, 2016):

$$\text{Langmuir: } m_{ad} = \rho_s \rho_{gsc} \frac{pV_L}{p + P_L} \tag{8}$$

$$\text{BET: } m_{ad} = \rho_s \rho_{gsc} \frac{V_m C p_r}{1 - p_r} \left[\frac{1 - (n+1) p_r^n + n p_r^{n+1}}{1 + (C-1) p_r - C p_r^{n+1}} \right]$$
$$p_r = \frac{p}{P_s},\ P_s = \exp(7.7437 - \frac{1306.5485}{19.4362 + T}) \tag{9}$$

where V_L is the Langmuir volume, L^3/M. P_L is the Langmuir pressure, $M/L/T^2$. ρ_s is the density of rock bulk matrix M/L^3, V_L is the Langmuir volume (the maximum adsorption capacity at a given temperature), L^3/M. P_L is the Langmuir pressure (the pressure at which the adsorbed gas volume is equal to $V_L/2$), $M/L/T^2$. V_m is the BET adsorption volume, L^3/M. C is the BET adsorption constant, dimensionless. n is the BET adsorption molecular layers, dimensionless. p_s is the pseudo-saturation pressure, $M/L/T^2$. Noted that, the unit of P_s is MPa.

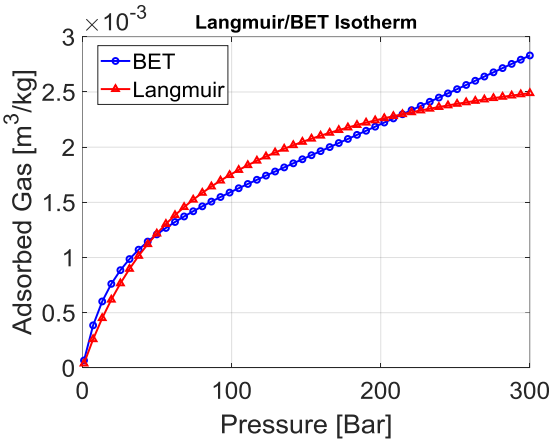

Fig. 6 Langmuir and BET isotherms curve with V_L=0.0031 m^3/kg and P_L=7.89 MPa, T=327.59 K, P_s=53.45 MPa, V_m=0.0015 m^3/kg, C=24.56 and n=4.46

Slippage flow & Diffusion: Considering slippage and diffusion effect of shale gas flow in the matrix, the apparent permeability in the low-pressure region around the fracture will be increased. In the MRST-Shale, the Florence's (2007) permeability correction factor (**Fig. 4**) is implemented as follows:

$$F_{app} = (1 + \alpha K_n)(1 + \frac{4K_n}{1 + K_n}) \tag{10}$$

$$K_n = \frac{\mu_g}{2.8284 p_g} \sqrt{\frac{\pi RT}{2M} \frac{\phi}{k_0}}$$
$$\alpha = \frac{128}{15\pi^2} \tan^{-1}(4K_n^{0.4}) \tag{11}$$

where Kn is the Knudsen number, dimensionless. α is the rarefaction parameter, dimensionless.

Non-Darcy Flow: In case of high flow velocity in the hydraulic fractures, the linear Darcy flow may no longer applicable. The permeability correction factor (Barree and Conway, 2004) for Darcy-Forchheimer flow can be expressed as follows:

$$F_{app} = \frac{2}{1+\sqrt{1+4\rho_g \beta \left(\frac{k_0}{\mu_g}\right)^2 |\nabla p|}} \tag{12}$$

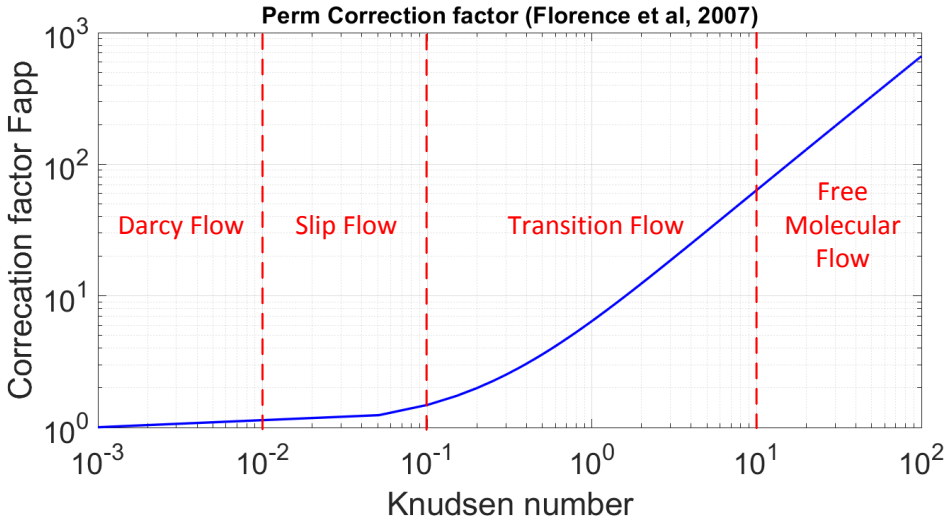

Fig. 7 – Permeability correction factor F_{app} versus Knudesen number for all flow regions with methane properties in Table 2, T=191 K, k_0=1e-10 and ϕ=0.1

where β is the empirical Forchheimer coefficient, for propped hydraulic fractures, which can be evaluated as follows (Rubin, 2010):

$$\beta = 3.2808 \frac{1.485 \times 10^9}{(k_0 \times 10^{-15})^{1.021}} \tag{13}$$

2.3 Geomechanics effect

As shown in Fig. 2, shale reservoir has multi-scale fractures. The fracture conductivity will be decreased due to the proppant embedment and fracture closure under high stress concentration near the fracture (Akkutlu et al, 2018). Three-types fracture are defined based on their length scale, including hydraulic fracture (half-length 50-100 meters, aperture 1mm), natural fracture (half-length 1-20 m, aperture 0.1mm), micro-fracture (half-length < 1m, aperture <0.1 mm). In this paper, a new geomechanics model considering multi-scale fracture is proposed. The larger fracture, such as the hydraulic fracture and natural fracture are explicitly modeled using EDFM. The micro-fractures are assumed highly connected and thus upscaled into the matrix permeability.

To consider the micro-fracture closure, Gangi's (1978) empirical pressure-dependent permeability reduction model can be applied as follows:

$$k = k_0 F_{app} = k_0 \left[1 - \left(\frac{P_c - \alpha_B p}{P_1} \right)^m \right]^3 \tag{14}$$

Where α_B is the Biot's constant, P_c is the confining overburden pressure, P_1 is the effective stress when micro-fracture completely closed. m is a constant related to surface roughness.

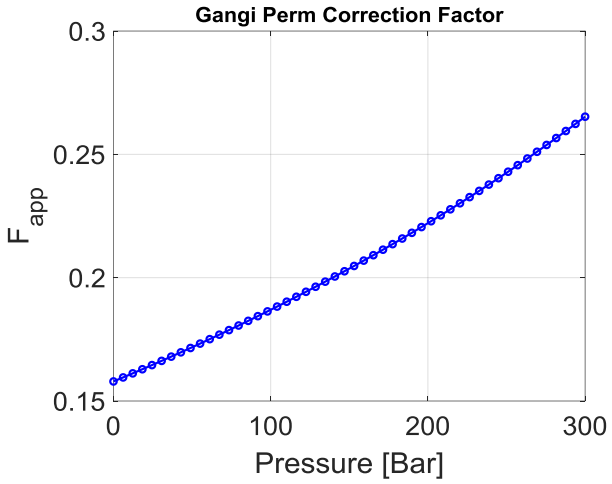

Fig. 8 – Permeability correction factor F_{frac} versus pore pressure with m=0.5, p_1=180 MPa, p_c=38 MPa and α=0.5

To consider the closure of hydraulic and natural fractures, Alramahi and Sundberg (2012) performed experiment to measure the effect of closure pressure on fracture conductivity for different shale samples from stiff shale to soft shale. The empirical model can be expressed as follows:

$$\begin{aligned} &\text{Stiff Shale: } F_{cd}(p) = \log(k_f w_f) = -0.0001\sigma(p) - 0.1082 \\ &\text{Meidum Shale: } F_{cd}(p) = \log(k_f w_f) = -0.0004\sigma(p) + 0.2191 \\ &\text{Soft Shale: } F_{cd}(p) = \log(k_f w_f) = -0.0006\sigma(p) - 0.4256 \\ &\sigma(p) = \sigma_h - p \end{aligned} \tag{15}$$

Where effective closure stress σ can be calculated by reservoir horizontal stress and in-situ fracture pore pressure. For hydraulic fracture, the fracture plane direction is normally orthogonal to the minimum horizontal stress and it support by rigid proppant, while for natural fracture has stochastic orientation and lacking support from proppant. Thus, the closure stress for hydraulic fracture and natural fracture can be expressed as follows:

$$\begin{aligned} &\text{HydraulicFrac: } \sigma_{HF} = \sigma_{h\min} - p \\ &\text{NaturalFrac: } \sigma_{NF} = \frac{\sigma_{h\min} + \sigma_{h\max}}{2} - p \end{aligned} \tag{16}$$

In the MRST-Shale, the fracture permeability can be reduced by a dynamic permeability correction factor as follows:

$$k_f = k_0 F_{app} = k_0 \frac{F_{cd}(p)}{F_{cd}(p_0)} \tag{17}$$

Currently, there is not experiment data available on the effect of closure pressure on the conductivity of natural fracture. So, as shown in **Fig. 9**, we used stiff shale correlation for hydraulic fracture but the soft shale correlation for the natural fracture to contrast the faster closure of the natural fracture.

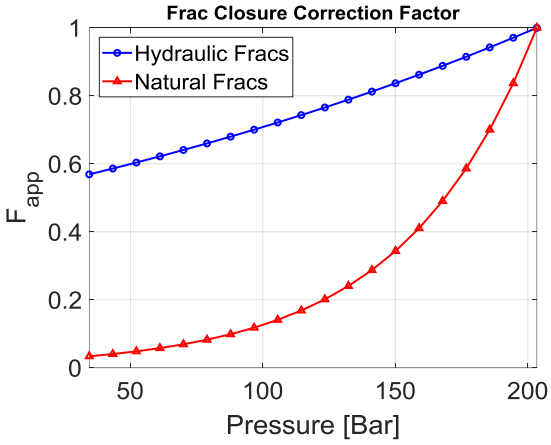

Figure 9 – Permeability correction factor F_{frac} for hydraulic fractures and natural fractures with p_o = 20.34 MPa and p_{wf} = 34.5 MPa $\sigma_{h\min}$ = 29 MPa and $\sigma_{h\max}$ = 34 MPa

3 Numerical Model

In this paper, a new shale gas simulation module is developed based on the automatic differentiation module (ad-core, ad-props), black-oil module (ad-blackoil) and hierarchical fracture model (hfm) module in open-source MATLAB Reservoir Simulation Toolbox (Lie, 2012). Two-point flux approximated finite volume method (TPFA-FVM) is applied for discretizing the governing equations (Eq. 3). Time discretization is implemented using a fully implicit first-order backward scheme. The corresponding Jacobian matrix from solving the nonlinear system is evaluated by automatic differentiation module of MRST-AD. All nonlinear functions by shale gas transport and storage mechanisms as well as geomechanics effect are defined as separate function. The overall implementation structure is shown as follows:

3.1 Numerical discretization

The discretized governing equation for 2D matrix system can be expressed as follows:

$$\frac{\phi V}{\Delta t}\left(b_g(p^{n+1})-b_g(p^n)\right)+\frac{(1-\phi)V}{\Delta t}\frac{1}{\rho_{gsc}}\left(m_{ad}(p^{n+1})-m_{ad}(p^n)\right)$$
$$-\mathbf{div}\left(b_g(p^{n+1})\frac{\prod_i F_{app,i}(p^{n+1})}{\mu_g(p^{n+1})}T\cdot\mathbf{grad}(p^{n+1})\right) \tag{18}$$
$$-Vb_g(p^{n+1})q_w(p^{n+1})-Vb_g(p^{n+1})\psi_{f-m}(p^{n+1})=0$$

The discretized governing equation for each 1D fracture system can be expressed as follows:

$$\frac{\phi V}{\Delta t}\left(b_g(p^{n+1})-b_g(p^n)\right)$$
$$-\mathbf{div}\left(b_g(p^{n+1})\frac{\prod_i F_{app,i}(p^{n+1})}{\mu_g(p^{n+1})}T\cdot\mathbf{grad}(p^{n+1})\right) \tag{19}$$
$$-Vb_g(p^{n+1})q_w(p^{n+1})-Vb_g(p^{n+1})\psi_{m-f}(p^{n+1})=0$$

where V is the bulk volume of a grid cell. To simplify the implementation of governing equations (Eqs. 18-19), three discrete domain delta δ functions for matrix (Ω_m), hydraulic fractures (Ω_{HF}) and natural fractures (Ω_{NF}) can be defined as follows:

$$\delta_m(x)=\begin{cases}1 & x\in\Omega_m\\ 0 & x\notin\Omega_m\end{cases},\quad \delta_{HF}(x)=\begin{cases}1 & x\in\Omega_{HF}\\ 0 & x\notin\Omega_{HF}\end{cases},\quad \delta_{NF}(x)=\begin{cases}1 & x\in\Omega_{NF}\\ 0 & x\notin\Omega_{NF}\end{cases} \tag{20}$$

A generic numerical model for fractured reservoir can be expressed as follows:

$$\frac{\phi V_{ijk}}{\Delta t}\left(b_g(p^{n+1})-b_g(p^n)\right)+\delta_m\frac{(1-\phi)V_{ijk}}{\Delta t}\frac{1}{\rho_{gsc}}\left(m_{ad}(p^{n+1})-m_{ad}(p^n)\right)$$
$$-\mathbf{div}\left(b_g(p^{n+1})\frac{\prod_i\left[1+\delta_{HF/NF,i}F_{app,i}(p^{n+1})\right]}{\mu_g(p^{n+1})}T\cdot\mathbf{grad}(p^{n+1})\right) \tag{21}$$
$$-V_{ijk}b_g(p^{n+1})q_w(p^{n+1})-V_{ijk}b_g(p^{n+1})\psi_{f-m/m-f}(p^{n+1})=0$$

Assuming vertical well fully penetrate the reservoir thickness, a semi-analytical Peaceman well model for a vertical well can be expressed as follows (Peaceman, 1983):

$$q_w=WI/\mu_g(p_{bh}-p)$$
$$WI=\frac{2\pi\Delta z\sqrt{k_{11}k_{22}}}{(\ln(r_e/r_w)+s)}\quad r_e=0.28\frac{(k_{11}\Delta y^2+k_{22}\Delta x^2)^{1/2}}{\sqrt{k_{11}}+\sqrt{k_{22}}} \tag{22}$$

where p_{bh} is the bottom hole pressure of a wellbore, M/L/T^2. Δx,y,z are the unit gridblock length in the x, y and z direction, L. h is the unit fracture cell length, L. r_w is the wellbore radius, L. k_{11} and k_{22} is the rock permeability on the x and y direction, L^2.

The solution matrix from Eqs. 21 can be expressed as follows:

$$\begin{bmatrix} \mathbf{A}_{mm} & \mathbf{A}_{mf} & \mathbf{A}_{mw} \\ \mathbf{A}_{fm} & \mathbf{A}_{ff} & \mathbf{A}_{fw} \\ \mathbf{A}_{wm} & \mathbf{A}_{wf} & \mathbf{A}_{ww} \end{bmatrix} \begin{Bmatrix} \mathbf{p}_m \\ \mathbf{p}_f \\ \mathbf{p}_w \end{Bmatrix} = \begin{Bmatrix} \mathbf{Q}_m \\ \mathbf{Q}_f \\ \mathbf{Q}_w \end{Bmatrix} \tag{23}$$

$$\#\mathbf{p}_m = \#\,\text{MatrixEles},\quad \#\mathbf{p}_f = \#\,\text{FractureEles},\quad \#\mathbf{p}_w = \#\text{Eles has well}$$

Noted that the shale gas viscosity, density and permeability corrections terms are all depends on solution variables. To solve non-linear system of Eq. 23, the residual form of Newton's iterations can be expressed as follows:

$$\mathbf{J}(\mathbf{x}^i)(\mathbf{x}^{i+1}-\mathbf{x}^i) = \frac{d\mathbf{R}}{d\mathbf{x}}(\mathbf{x}^i)(\mathbf{x}^{i+1}-\mathbf{x}^i) = -\mathbf{R}(\mathbf{x}^i) \tag{24}$$

The Jacobian matrix **J** is calculated by automatic differentiation in MRST.

3.2 EDFM

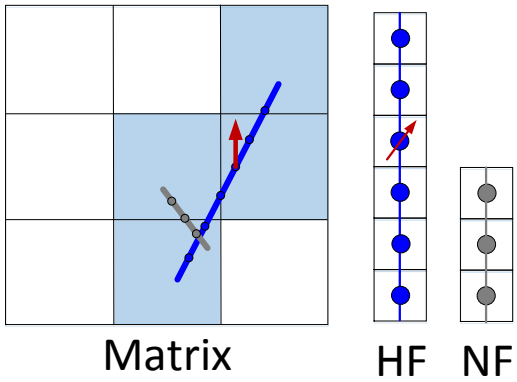

Fig. 10 – Grid system in EDFM for matrix, natural fracture and hydraulic fracture

As shown in **Fig. 10**, EDFM adopted the concept of dual-continuum fracture modeling method, the mass transfer term $\psi_{f-m/m-f}$ is introduced to couple the solution among matrix and fractures. Thus, the matrix grid is not necessary align with the fracture plane. As shown in **Fig. 11**, there are three kinds of non-neighbor connection (NNC) in EDFM formulation: 1) fracture-matrix connectivity, 2) fracture-fracture connectivity and 3) fracture-well connectivity. The general NNC model can be expressed as follows (Xu, 2015):

$$\psi_{f-m}^{NNC} = T_{f-m}^{NNC}(p_f^{n+1} - p_m^{n+1})$$
$$\psi_{f-m}^{NNC} = -\psi_{m-f}^{NNC} \tag{25}$$

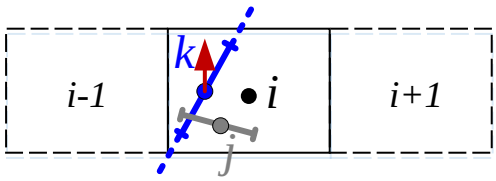

Unit EDFM System

Fig. 11 – Unit EDFM NNCs of 1) fracture-matrix (*i*-*k* pair) connectivity 2) fracture-fracture (*j*-*k* pair) connectivity and 3) fracture-wellbore (cell *k*) connectivity

Fracture-matrix NNC: The fracture-matrix transmissibility ($T_{f\text{-}m}$) can be expressed as follows:

$$T_{ik}^{NNC} = \frac{k_{0,ik}}{\mu_{g,ik}} \frac{A_{ik}}{\langle d \rangle_{ik}} \tag{26}$$

where $A_{i,k}$ is the intersection area fraction between a fracture plane and a gridblock. For 2D grid, the area is the product of intersection fracture cell length and matrix gridblock thickness. Noted that the harmonic average for the permeability and upwind value for viscosity. $\langle d \rangle_{i,k}$ is the average normal distance between matrix cell and fracture plane, which can be calculated as follows:

$$\langle d \rangle_{ik} = \frac{\int d_{ik} dv}{V_i} \tag{27}$$

For 2D structured grid, an analytical solution is available for the average normal distance (Tene et al, 2016).

Fracture-fracture NNC: the star-delta transformation can be used to calculate the transmissibility between intersected fractures as follows (Hajibeygi et al, 2011):

$$T_{jk}^{NNC} = \frac{t_j t_k}{\sum_{m=1}^{N_{ints}} t_m}, \; t_m = \frac{A_{f,m}}{0.5 h_{f,m}} \frac{k_{0,m}}{\mu_{g,m}} \tag{28}$$

where A_f is the cross-section area of fracture plane, h_f is the fracture cell length.

Fracture-well NNC: If a well intersected with a fracture cell, similar to Peaceman well model of Eq. 22. The effective wellbore index (WI) and equivalent radius (r_e) can be expressed as follows (Xu, 2015):

$$WI_f = \frac{2\pi k_f w_f}{\ln(r_e / r_w)}, \; r_e = 0.14\sqrt{h_f^2 + \Delta z^2} \tag{29}$$

4 Verification

To verify the presented EDFM shale gas model, two numerical simulation are performed against a commercial simulator (CMG, 2015) and an in-house simulator with unstructured mesh (Jiang and Younis, 2015). The base model and simulation parameters for all cases as shown in **Table 2**:

Table 2—Base model and simulation parameters for all cases

Property	Unit	Value
Rock density	kg/m^3	2500
Molecular weight, CH_4	kg/mol	0.01604
Critical pressure, CH_4	MPa	4.64
Critical temperature, CH_4	K	191
Well radius	m	0.1

4.1 Case 1 – Verification of fully implicit black-oil solution

MRST-Shale is firstly verified in a simple case against a commercial simulator (CMG) with a single vertical hydraulic fracture. In this simulation, the empirical Z-factor (Eq. 5) model and Langmuir adsorption (Eq. 8) is used. The detailed reservoir and fluid properties can be found in **Fig. 12** and **Table 3**.

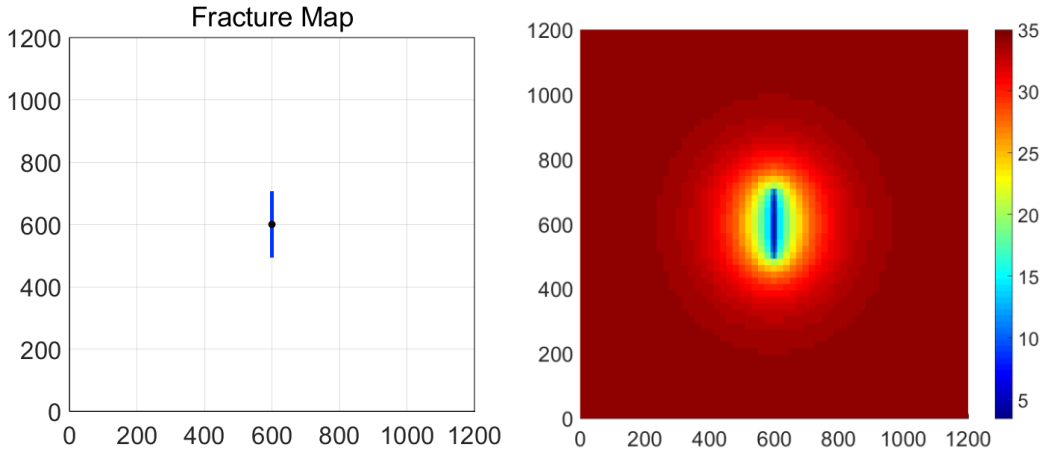

(a) (b)

Fig. 12 Fracture map (a) and pressure contour after 30 years (b) of the Case 1

Table 3. Key reservoir and simulation parameters of Case 1

Property	Unit	Value
Domain dimensions (x,y)	m	1200,1200
Formation thickness	m	45.72
Initial reservoir pressure	MPa	34.47
Temperature	K	327.60
Langmuir pressure	MPa	8.9632

Langmuir volume	m^3/kg	0.00396
Matrix porosity		0.07
Matrix compressibility	1/Pa	1.45e-10
Matrix permeability	nD	500
Fracture permeability	mD	500
Fracture width	m	0.003
Fracture half-length	m	106.68
Fracture conductivity	md-ft	50
Well BHP	MPa	3.45
Production time	years	30

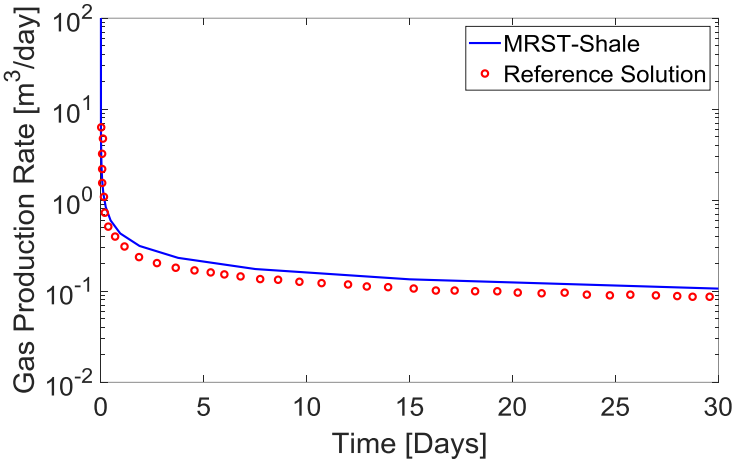

I'm working on benchmarking this problem now.

4.2 Case 2 – Verification of transport mechanism and irregular fracture shape

MRST-Shale is then verified against an in-house simulator (Jiang and Younis, 2015) by considering more complex fracture geometry and transport mechanisms. For the reference solution, it used fully unstructured mesh with LGR to capture the complex fracture geometry as well as the sharp pressure gradient near the fracture. By considering transport and storage mechanisms, the gas rate solution of two sub-case are investigated. In this first sub-case, full storage and transport mechanism with Langmuir adsorption (Eq. 8) and slippage & diffusion flow (Eq. 10) is considered. In the second sub-case, only PR-EOS (Eq. 6) and Lee's natural gas viscosity model (Eq. 7) is considered, but the shale gas transport and storage mechanism is ignored. The detailed fracture map and simulation parameters for the case 2 are elaborated in **Table 3**.

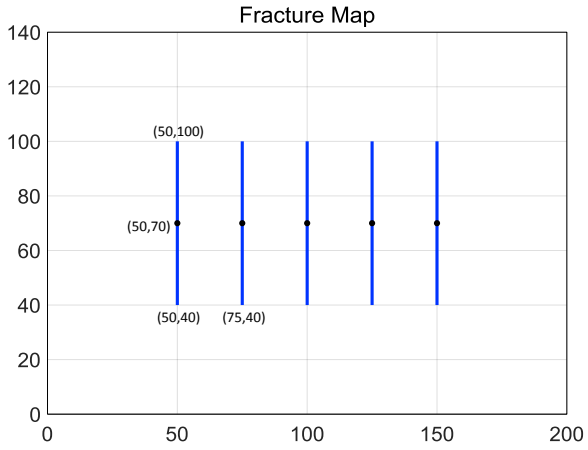

Fig. 12 Fracture map of case 2

Table 3. Key reservoir and simulation parameters of case 2

Property	Unit	Value
Domain dimensions (x,y)	m	200,140
Formation thickness,	m	10
Initial reservoir pressure	MPa	16
Temperature	K	343.15
Langmuir pressure	MPa	4
Langmuir volume	m^3/kg	0.018
Matrix porosity		0.1
Matrix compressibility	1/Pa	1.0e-9
Fracture porosity		1.0
Matrix permeability	nD	100
Fracture permeability	D	1
Fracture width	m	1e-3
Well BHP	MPa	4
Production time	days	10000

Other parameters are the same as in Table 2

As shown in

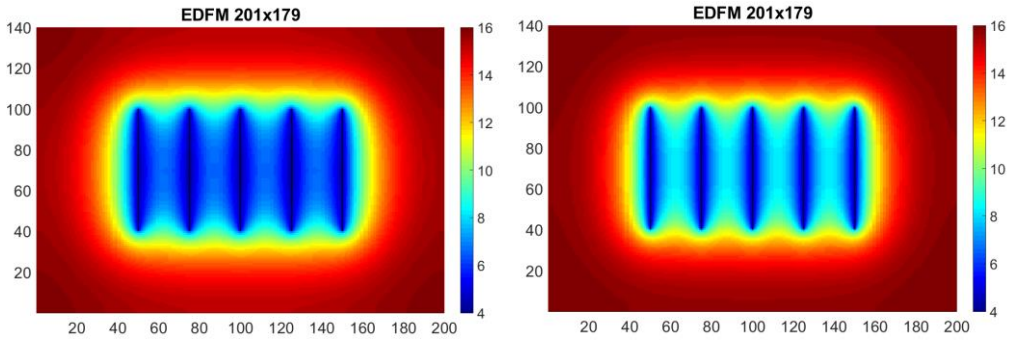

Full mechanism

No mechansim

Fig. 12 Pressure contour with and without full shale gas transport mechanism @ 2500 days of case 2

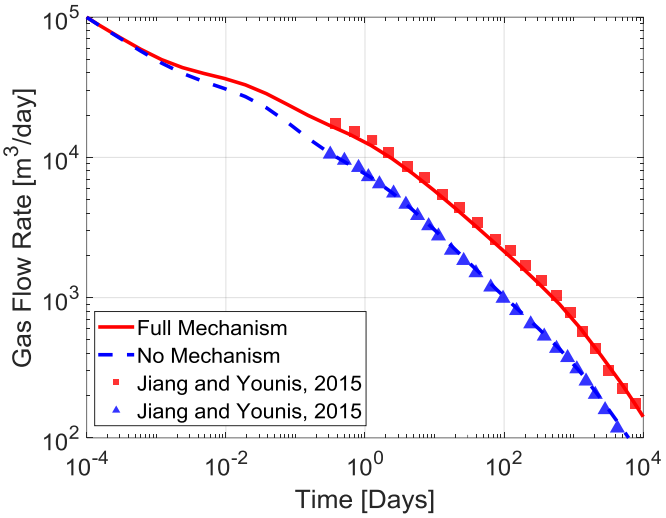

Fig. 13 Comparison of Log-Log gas flow rate for case 2 between MRST-Shale and in-house simulator (2015)

5 Application

5.1 Case 3: History matching and production forecast

To further verify the applicability of the MRST-Shale. A history matching with field production data on a Barnett shale has performed. The field production and simulation data are adopted from literature (Cao, Liu and Leong, 2016; Yu and Kamy Sepehrnoori, 2014). The detailed reservoir and fluid parameters are shown as in **Fig. 14** and **Table 4**.

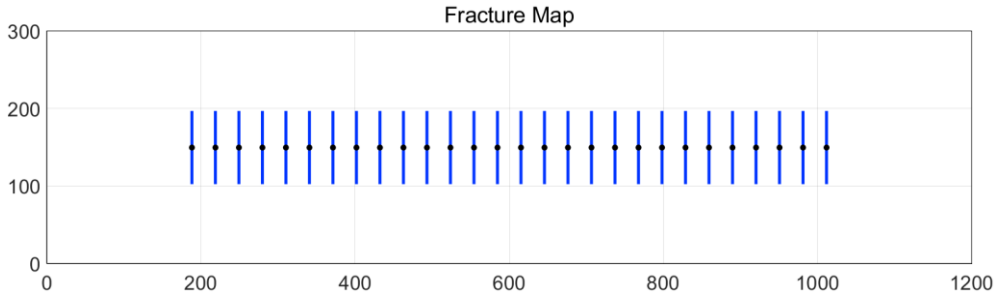

Fig. 14 Fracture map with 28 planar hydraulic fractures of Case 3

Table 4. Key reservoir and simulation parameters of Barnet shale for Case 3 (Cao, 2016)

Property	Unit	Value
Domain dimensions (x,y)	m	1200,300
Depth	m	5463
Formation thickness,	m	90

Initial reservoir pressure	MPa	20.34
Temperature	K	352
Rock density	kg/m^3	2500
Langmuir pressure	MPa	4.47
Langmuir volume	m^3/kg	0.00272
Matrix porosity		0.03
Matrix compressibility	1/Pa	1.5e-10
Fracture compressibility	1/Pa	1.0e-8
Matrix permeability	nD	200
Fracture permeability	mD	100
Fracture width	m	0.003
Fracture spacing	m	30.5
Fracture half-length	m	47.2
Fracture conductivity	md-ft	1
Well BHP	MPa	3.69
Production time	days	1600

Other parameters are the same as in Table 2

In this simulation, a rectangle reservoir with dimension of 1100 × 290 × 90 m was discretized by 148 × 39 × 1 grids. 28 stages hydraulic fractures in the center of domain with the half-length of 47.2 m and the fracture spacing of 30.5 m. The fractures are assumed have constant aperture of 0.003 m and permeability of 100 md. Only shale gas storage mechanism of Langmuir adsorption (Eq. 8) is considered. **Fig. 15** shows the pressure contour at different production time (400 days and 1600 days). **Fig. 16** shows the comparison of production rate between MRST-Shale and field data which shows good agreements with the field production data. Based on matched simulation parameters, the production forecast can be easily performed as in Fig. 21.

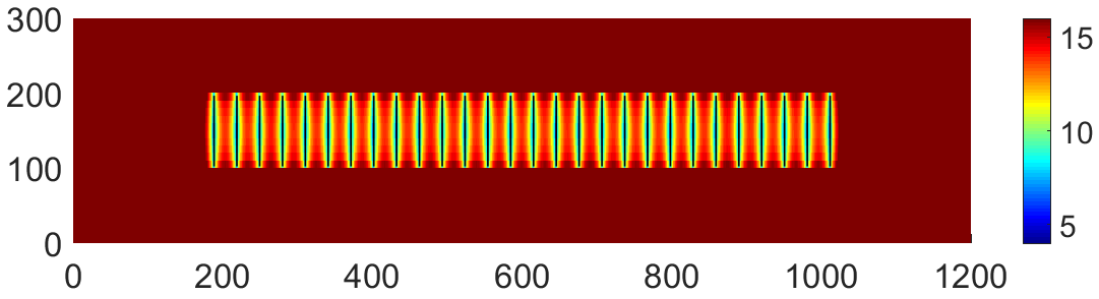

(a) 400 days

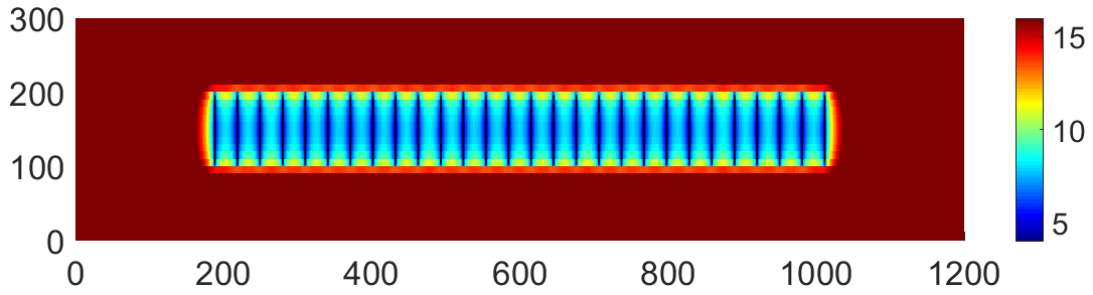

(b) 1600 days

Figure 15 Pressure contour at (a) 400 days and (b) 1600 days for Barnett shale reservoir (case 3)

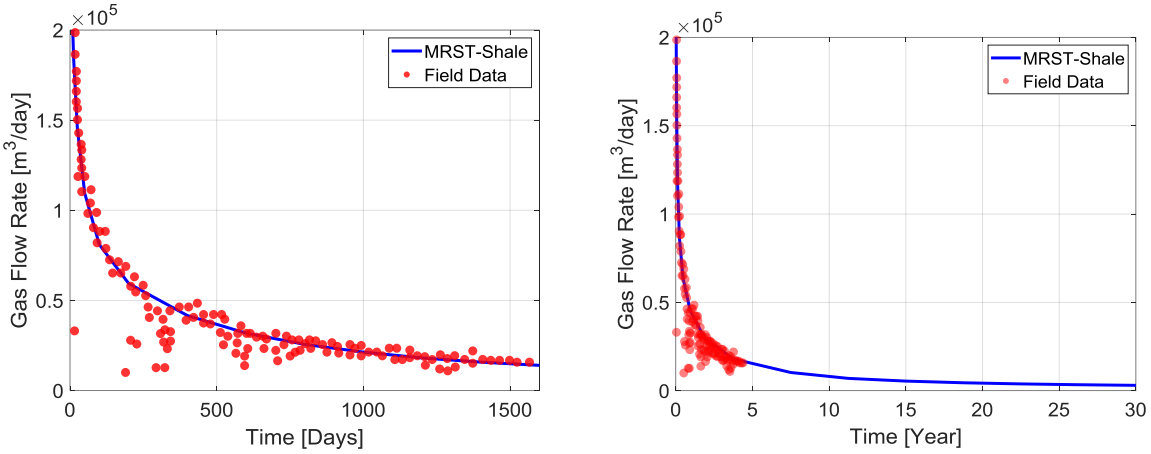

Fig. 16 History matching (left) and production forecast (right) of a Barnett shale well.

5.2 Case 4: New model evaluation

To illustrate the capability of modular design and rapid prototyping of MRST-Shale, a new shale gas model considering geomechanics effect (Eqs. 15-17) for multi-scale fractured network is implemented and evaluated using MRST-Shale. In this section, the influence of multi-scale fracture network and geomechanics effect on shale gas production performance will be investigated.

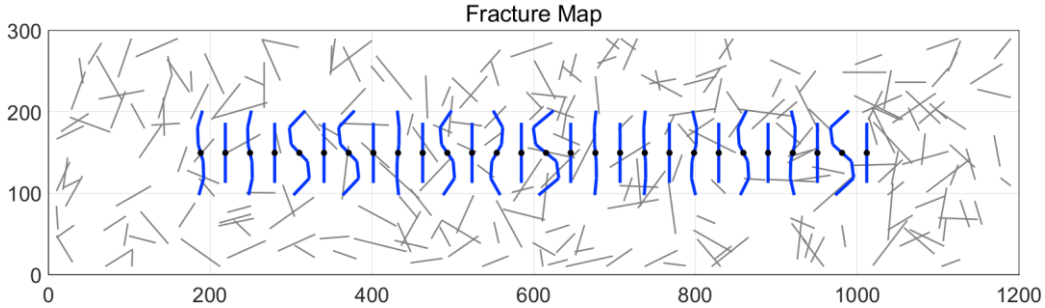

Fig. 17 Fracture map with 28 non-planar hydraulic fractures and 248 natural fractures of Case 4

In this case, all the simulation parameters are the same with Case 3 of Barnett shale reservoir. The total length of non-planar hydraulic fractures (blue lines in **Fig. 17**) is the same as planar fractures used in Case 3 (blue lines in Fig. 14). Natural fractures are stochastically generated by using an open-source fracture generator ADFNE (Alghalandis, 2017). The geomechanics parameters for shale reservoir are assumed (Wasaki and Akkutlu, 2015) as follows (**Table 5**):

Table 5. Geomechanics parameters of Barnet shale for Case 4

Property	Unit	Value
Biot constant, α	-	0.5
Overburden confining stress, p_c	MPa	38
Maximum horizontal stress, s_{hmax}	MPa	34
Minimum horizontal stress, s_{hmin}	MPa	29
Maximum closure stress for micro-fracture, p_1	MPa	180
Gangi exponential constant, m	-	0.5

Other parameters are the same as in Tables 2-3

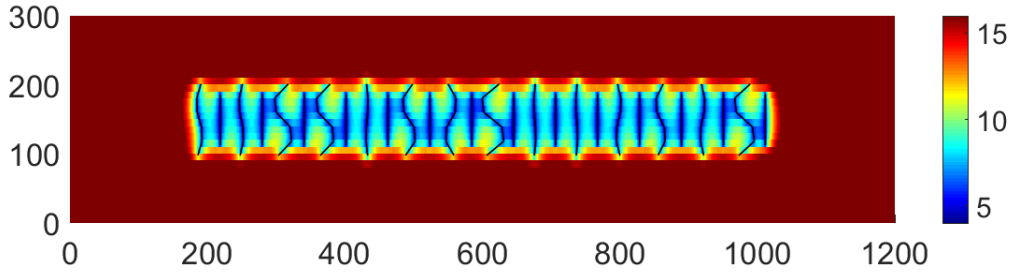

(a) Non-planar hydraulic fracture (Same total fracture length with Case 3)

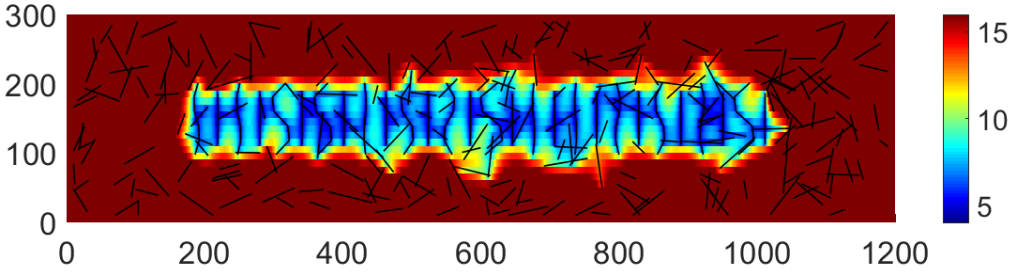

(b) Non-planar hydraulic fracture + natural fractures

Fig. 18 Pressure contour at 3.75 years for Barnett shale reservoir with Non-planar fracture geometry and natural fractures (case 4)

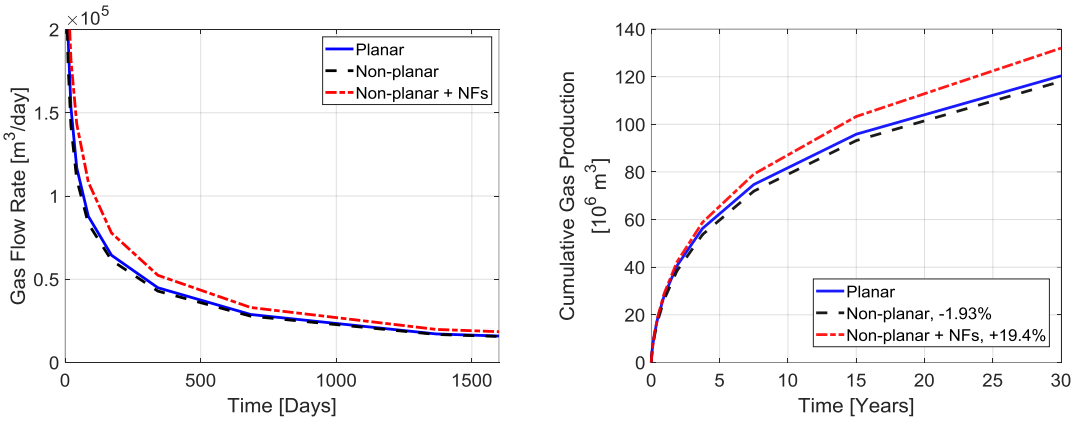

Fig. 19 Comparison of gas flow rate (left) and cumulative production (right) between Planar, Non-Planar and Non-Planar & natural fractures cases

Firstly, the effect of complex fracture network on well performance is studied. **Fig 18** shows the pressure contour for the non-planar fractures with and without the natural fractures. Obviously, the case of natural fractures has larger and better stimulated reservoir volume (SRV). Thus, as shown in **Fig. 19**, the cumulative gas production of non-planar case with natural fracture has much higher value (19.4% improvements) than the planar case in the Case 3. While in the case of same total length, the non-planar fracture geometry will slightly degenerate the well performance (-1.9% reduction). Jiang and Younis (2015) arrives the similar conclusions about this.

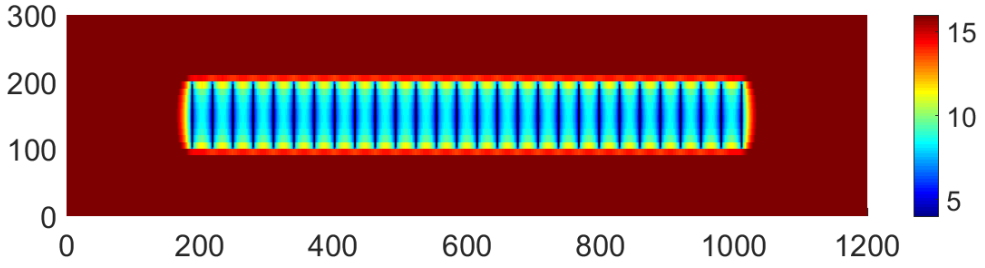

(a) Planar hydraulic fracture (Same with Case 3)

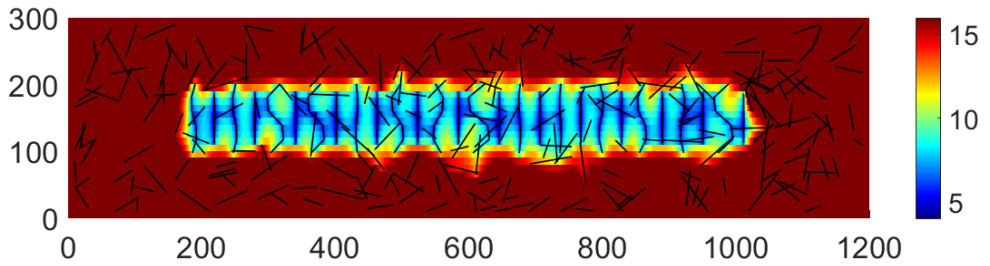

(c) Realistic: Non-planar hydraulic fracture + natural fractures + geomechanics effect

Fig. 20 Pressure contour at 3.75 years for Barnett shale reservoir with planar hydraulic fractures case and realistic case

The influence of geomechanics effect with fracture closure on well performance is further investigated by implementing **Eqs. 15-17**. **Fig. 20** shows the pressure contour at the 3.75 years for the planar case (Fig. 20a) and realistic case (Fig. 20b) with non-planar hydraulic fracture, natural fractures and geomechanics effect. As shown in **Fig. 21a**, at the earlier production period**,** both planar case and realistic case matches well with the field data. But in the later production time, the realistic case with natural fractures has 9.67% higher cumulative production than the simple planar case. Thus, the modeling of natural fractures and geomechanics effect is important for long-term production evaluation. Ignoring natural fractures and geomechanics effect will greatly underestimating the well performance.

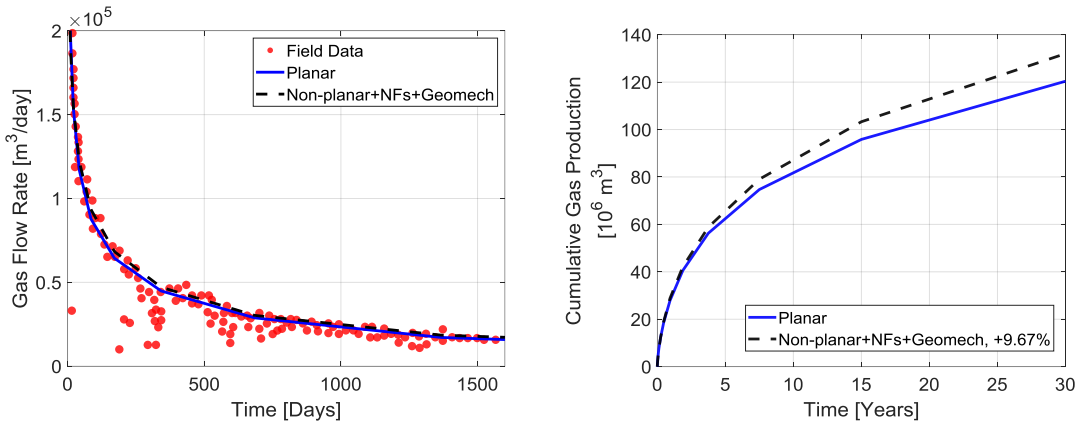

Fig. 21 Comparison of gas flow rate (left) and cumulative production (right) between planar hydraulic fracture case and realistic case with non-planar, natural fractures and geomechanics effect

6 Conclusion

In this work, A generic shale gas model and an open-source simulator MRST-Shale are developed for shale gas simulation with state-of-art flow and storage mechanics. It is verified against commercial and in-house reservoir simulators. Also, a field application of history matching and production forecasting are successful performed. Several conclusions can be drawn as follows:

(1) A generic shale gas numerical model is developed which can be used to model any state-of-art storage and transport mechanisms, including gas adsorption, gas slippage & diffusion, non-Darcy flow as well as geomechanics effect by considering complex multi-scale fracture geometries.

(2) Based on the proposed numerical model, a general and open-source simulator, MRST-Shale is developed. With the help of the fracture generator, automatic differentiation, discrete differential operators and object-designed framework of MRST-Shale, it can easily model non-linear, pressure-dependent and rock properties-dependent shale gas problem with complex fracture geometry.

(3) MRST-Shale are verified against commercial and in-house simulator. A field application of

history matching and production forecast are also successfully performed with complex natural fracture and new geomechanics model. Results shows that the natural fracture and fracture closure have significant impact (over 10%) on the long-term cumulative gas production. Ignoring natural fracture and fracture closure will underestimating and overestimating the long-term well performance, respectively.

(4) MRST-Shale is capable of serving as an efficient, flexible research tool to evaluate new models with arbitrary non-linearity and fracture complexity. It can serve as a bridge between mechanism study and field scale engineering application.

Nomenclature

ρ_g = mass density of natural gas, kg/m^3
ϕ = absolute rock porosity, dimensionless
Ω_m = matrix domain
Ω_f = fracture domain
m_{ad} = storage mechanism term, kg/m^3
F_{app} = transport mechanism term, dimensionless
k_0 = absolute Darcy rock permeability, m^2
μ_g = viscosity of natural gas, Pa·s
p = pore pressure, Pa
q_w = volumetric sink/source term, m^3/day
b_g = inverse formation volume factor, dimensionless
M = molecular weight of natural gas, kg/mol
Z = compressibility factor of natural gas, dimensionless
R = ideal gas constant, 8.314 J/(mol·K)
T = reservoir temperature, K
T_{pr} = pseudo-temperature for natural gas, dimensionless
T_c = critical-temperature for natural gas, K
p_{pr} = pseudo-pressure for natural gas, dimensionless
p_c = critical-pressure for natural gas, Pa
$a_{0,1,2}$ = constants for Peng-Robinson equation of state, dimensionless
a,b = constants for Peng-Robinson equation of state, dimensionless
A,B = constants for Peng-Robinson equation of state, dimensionless
K,X,Y=constants for Lee-Conzalez-Eakin natural gas viscosity, dimensionless
ρ_s = mass density of bulk matrix, kg/m^3
ρ_{gsc} = mass density of natural gas at the standard condition, kg/m^3
V_L = Langmuir volume, m^3/kg
P_L = Langmuir pressure, Pa
V_m = BET volume, m^3/kg
P_s = BET pseudo-saturation pressure, Pa
p_r = psdueo-pressure for BET isotherm, dimensionless
C = constant for BET isotherm, dimensionless
n = constant for BET isotherm, dimensionless
α = rarefaction coefficient for gas slippage flow, dimensionless

K_n = Knudsen number, dimensionless
β = Darcy-Forchheimer coefficient, dimensionless
α_B = Biot's coefficient, dimensionless
P_c = reservoir confining overburden pressure, Pa
P_1 = reservoir effective stress when micro-fracture completely closed, Pa
m = constant for the Gangi's model, Pa
F_{cd} = fracture conductivity, md·ft
p_0 = initial reservoir pressure, m
σ = effective fracture closure stress, Pa
σ_{hf} = effective closure stress for hydraulic fracture, Pa
σ_{nf} = effective closure stress for natural fracture, Pa
σ_h = reservoir horizontal principle stress, Pa
σ_{hmin} = minimum reservoir horizontal principle stress, Pa
σ_{hmax} = maximum reservoir horizontal principle stress, Pa
k_f = absolute Darcy permeability of fracture, m^2
w_f = fracture width, m
V = bulk volume of a grid cell, m
δ = discrete domain delta function, dimensionless
Δt = solution time-step, day
$\psi_{f\text{-}m}$ = mass coupling term for matrix, dimensionless
$\psi_{m\text{-}f}$ = mass coupling term for fracture, dimensionless
p_{bh} = wellbore bottom hole pressure, Pa
k_{11} = absolute Darcy rock permeability in x-direction, m^2
k_{22} = absolute Darcy rock permeability in y-direction, m^2
r_e = equivalent radius for wellbore model, m
r_w = wellbore radius, m
s = wellbore skin factor, dimensionless
Δx = grid cell size in x-direction, m
Δy = grid cell size in y-direction, m
Δz = grid cell size in z-direction, m
WI = wellbore index, dimensionless
$\boldsymbol{x}$ = Unknown vector, -
$\boldsymbol{J}$ = Jacobian matrix, -
$\boldsymbol{R}$ = Residual vector, -
WI = wellbore index, dimensionless
p_f = pore pressure at the fracture domain, Pa
p_m = pore pressure at matrix domain, Pa
T = transmissibility, dimensionless
A = intersection area among fracture and matrix, m^2
d = average normal distance among fracture and matrix, m
h_f = length of a fracture cell, m
t = fracture transmissibility for fracture-fracture NNC, dimensionless

Subscripts:

NF = natural fracture
HF = hydraulic fracture
m = matrix
f = fracture
g = gas
w = well

References

Akkutlu IY, Fathi E. Multi-scale gas transport in shales with local kerogen heterogeneities. SPE J. 2012;17(4):1002–1011.

Alghalandis, Y.F., 2017. ADFNE: Open source software for discrete fracture network engineering, two and three dimensional applications. Computers & Geosciences, 102, pp.1-11.

Akkutlu, I.Y., Efendiev, Y., Vasilyeva, M. and Wang, Y., 2018. Multiscale model reduction for shale gas transport in poroelastic fractured media. Journal of Computational Physics, 353, pp.356-376.

Alramahi, B. and Sundberg, M.I., 2012, January. Proppant embedment and conductivity of hydraulic fractures in shales. In 46th US Rock Mechanics/Geomechanics Symposium. American Rock Mechanics Association.

Civan F. Effective correlation of apparent gas permeability in tight porous media. Transp Porous Media. 2010;82(2):375–384.

Civan F, Rai CS, Sondergeld CH. Shale-gas permeability and diffusivity inferred by improved formulation of relevant retention and transport mechanisms. Transp Porous Media. 2011;86(3):925–944.

Cao, P., Liu, J. and Leong, Y.K., 2016. A fully coupled multiscale shale deformation-gas transport model for the evaluation of shale gas extraction. Fuel, 178, pp.103-117.

Chen Z, Liao X, Zhao X, Lyu S, Zhu L. A comprehensive productivity equation for multiple fractured vertical wells with non-linear effects under steady-state flow. J Pet Sci Eng. 2017; 149:9–24.

Elliott, J.R. and Lira, C.T., 2011. Introductory chemical engineering thermodynamics (Vol. 184). Upper Saddle River, NJ: Prentice Hall PTR.

Florence, F.A., Rushing, J., Newsham, K.E. and Blasingame, T.A., 2007, January. Improved permeability prediction relations for low permeability sands. In Rocky Mountain Oil & Gas Technology Symposium. Society of Petroleum Engineers.

Gangi, A.F., 1978, October. Variation of whole and fractured porous rock permeability with confining pressure. In International Journal of Rock Mechanics and Mining Sciences & Geomechanics Abstracts (Vol. 15, No. 5, pp. 249-257). Pergamon.

Hajibeygi, H., Karvounis, D. and Jenny, P., 2011. A hierarchical fracture model for the iterative multiscale finite volume method. Journal of Computational Physics, 230(24), pp.8729-8743.

Javadpour F, Fisher D, Unsworth M. Nanoscale gas flow in shale gas sediments. J Can Pet Technol. 2007;46(10):55–61.

Jiang, J. and Younis, R.M., 2015. Numerical study of complex fracture geometries for unconventional gas reservoirs using a discrete fracture-matrix model. Journal of Natural Gas Science and Engineering, 26, pp.1174-1186.

Klinkenberg, L.J., 1941, January. The permeability of porous media to liquids and gases. In Drilling and production practice. American Petroleum Institute.

Lie, K.A., Krogstad, S., Ligaarden, I.S., Natvig, J.R., Nilsen, H.M. and Skaflestad, B., 2012. Open-source MATLAB implementation of consistent discretisations on complex grids. Computational Geosciences, 16(2), pp.297-322.

Olorode, O., Freeman, C.M., Moridis, G. and Blasingame, T.A., 2013. High-resolution numerical modeling of complex and irregular fracture patterns in shale-gas reservoirs and tight gas reservoirs. SPE Reservoir Evaluation & Engineering, 16(04), pp.443-455.

Olorode, O., Akkutlu, I.Y. and Efendiev, Y., 2017. Compositional Reservoir-Flow Simulation for Organic-Rich Gas Shale. SPE Journal.

Peaceman, D.W., 1983. Interpretation of well-block pressures in numerical reservoir simulation with nonsquare grid blocks and anisotropic permeability. Society of Petroleum Engineers Journal, 23(03), pp.531-543.

Rubin B. Accurate simulation of non-darcy flow in stimulated fractured shale reservoirs. In: SPE 132093, presented at the SPE western regional meeting, Anaheim, CA; May 27-29, 2010

Sakhaee-Pour A, Bryant SL. Gas permeability of shale. SPE Reservoir Eval Eng. 2012;15(4):401–409.

Sandve TH, Berre I, Nordbotten JM. An efficient multi-point flux approximation method for discrete fracture–matrix simulations. J Comput Phys. 2012;231(9):3784–3800

Ţene, M., Al Kobaisi, M.S. and Hajibeygi, H., 2016. Algebraic multiscale method for flow in heterogeneous porous media with embedded discrete fractures (F-AMS). Journal of Computational Physics, 321, pp.819-845.

Wang FP, Reed RM. Pore networks and fluid flow in gas shales. In: SPE Annual Technical Conference and Exhibition. New Orleans, Louisiana, 2009.

Wasaki, A. and Akkutlu, I.Y., 2015. Permeability of organic-rich shale. SPE Journal, 20(06), pp.1-384.

Xu Y. Implementation and application of the Embedded Discrete Fracture Model (EDFM) for reservoir simulation in fractured reservoirs. Master Thesis, The University of Texas at Austin, 2015.

Yu, W., Xu, Y., Liu, M., Wu, K. and Sepehrnoori, K., 2018. Simulation of shale gas transport and production with complex fractures using embedded discrete fracture model. AIChE Journal, 64(6), pp.2251-2264.

Yu, W. and Sepehrnoori, K., 2014. Simulation of gas desorption and geomechanics effects for unconventional gas reservoirs. Fuel, 116, pp.455-464.

Yu, W., Sepehrnoori, K. and Patzek, T.W., 2016. Modeling gas adsorption in Marcellus shale with Langmuir and bet isotherms. SPE Journal, 21(02), pp.589-600.

Yang R, Huang Z, Yu W, Li G, Ren W, Zuo L, Tan X, Sepehrnoori K, Tian S, Sheng M. A comprehensive model for real gas transport in shale formations with complex non-planar fracture networks. Sci Rep. 2016; 6:36673.

Zhang Y, Yu W, Sepehrnoori K, Di Y. A comprehensive numerical model for simulating fluid transport in nanopores. Sci Rep. 2017;7: 40507.